TECHNICAL RESEARCH REPORT

Local Bifurcations in PWM DC-DC Converters

by C.-C. Fang, E. H. Abed

T.R. 99-5

ISR develops, applies and teaches advanced methodologies of design and analysis to solve complex, hierarchical, heterogeneous and dynamic problems of engineering technology and systems for industry and government.

ISR is a permanent institute of the University of Maryland, within the Glenn L. Martin Institute of Technology/A. James Clark School of Engineering. It is a National Science Foundation Engineering Research Center.

Web site http://www.isr.umd.edu

Report Documentation Page

Form Approved
OMB No. 0704-0188

1. REPORT DATE	2. REPORT TYPE	3. DATES COVERED
1999		**-**

4. TITLE AND SUBTITLE	5a. CONTRACT NUMBER
Local Bifurcations in PWM DC-DC Converters	5b. GRANT NUMBER
	5c. PROGRAM ELEMENT NUMBER
6. AUTHOR(S)	5d. PROJECT NUMBER
	5e. TASK NUMBER
	5f. WORK UNIT NUMBER
7. PERFORMING ORGANIZATION NAME(S) AND ADDRESS(ES) **Office of Naval Research,One Liberty Center,875 North Randolph Street Suite 1425,Arlington,VA,22203-1995**	8. PERFORMING ORGANIZATION REPORT NUMBER
9. SPONSORING/MONITORING AGENCY NAME(S) AND ADDRESS(ES)	10. SPONSOR/MONITOR'S ACRONYM(S)
	11. SPONSOR/MONITOR'S REPORT NUMBER(S)

12. DISTRIBUTION/AVAILABILITY STATEMENT
Approved for public release; distribution unlimited

13. SUPPLEMENTARY NOTES

14. ABSTRACT
see report

15. SUBJECT TERMS

16. SECURITY CLASSIFICATION OF:			17. LIMITATION OF ABSTRACT	18. NUMBER OF PAGES	19a. NAME OF RESPONSIBLE PERSON
a. REPORT	b. ABSTRACT	c. THIS PAGE			
unclassified	**unclassified**	**unclassified**		**23**	

Local Bifurcations in PWM DC-DC Converters

Chung-Chieh Fang and Eyad H. Abed*
Department of Electrical Engineering
and the Institute for Systems Research
University of Maryland
College Park, MD 20742 USA
ccfang@isr.umd.edu abed@isr.umd.edu

Manuscript: Jan. 25, 1999

Abstract

A general sampled-data model of PWM DC-DC converters [1, 2] is employed to study types of loss of stability of the nominal (periodic) operating condition and their connection with local bifurcations. In this work, the nominal solution's periodic nature is accounted for via the sampled-data model. This results in more accurate predictions of instability and bifurcation than can be obtained using the averaging approach. The local bifurcations of the nominal operating condition studied here are period-doubling bifurcation, saddle-node bifurcation, and Neimark bifurcation. Examples of bifurcations associated with instabilities in PWM DC-DC converters are given. In particular, input filter instability is shown to be closely related to the Neimark bifurcation.

1 Introduction

There have been many studies of instabilities of PWM DC-DC converters. For example, subharmonic oscillation has been studied in [3, 4, 5, 6, 7, 8, 9, 10]; input filter instability in [11, 12, 13]; chaos in [14, 15, 16, 6, 17, 18, 19]; and various other instabilities in [20, 21, 22, 23, 24, 25]. From a practical perspective, it is useful to classify instabilities depending on how and in what range of operating conditions they arise. Bifurcation theory is a tool that facilitates the study of loss of stability and its implications for system dynamical behavior. Upon loss of stability of a steady state solution of a dynamical system, typically a bifurcation occurs in which new steady states can arise. Thus, loss of stability of one steady state may lead to operation at a new steady state. A useful classification of bifurcations is that of local bifurcation vs. global bifurcation [26, 27]. In a local bifurcation, the original steady state is an equilibrium point or limit cycle. In a global bifurcation, the original steady state has some other structure (say, an almost periodic solution, or a chaotic orbit). In PWM DC-DC converters, the nominal operating condition is a periodic steady state, i.e., a limit cycle. Since this limit cycle has a small ripple, it is often approximated as an equilibrium point. This is true, for instance, in the averaging method. In this paper, local bifurcations of PWM DC-DC converters are studied without invoking this approximation. The focus on local bifurcations is due to the fact, from a practical point of view, that these bifurcations can be expected to arise before any global bifurcation.

*Corresponding author

The most popular approach for stability analysis of PWM DC-DC converters has been the averaging method [28, 29]. Here, the nominal periodic steady state of a PWM converter is averaged to an equilibrium. The periodic steady state in high switching operation has small amplitude (ripple), and averaging is therefore a reasonable approach. However, close to the onset of instability, the *periodic* nature of the steady state operating condition needs to be considered in order to obtain accurate results. Indeed, it has been reported [30, 31] that averaging leads to erroneous conclusions regarding the onset of instability.

This paper employs general sampled-data modeling [5, 32, 33, 34, 1, 2, 35] and analysis of DC-DC converters. The local bifurcations that typically occur in PWM DC-DC converters are studied. These are period-doubling bifurcation, saddle-node bifurcation, and Neimark bifurcation. Examples of instability in PWM DC-DC converters are used to illustrate these bifurcations. In particular, input filter instability is shown to be closely related to the Neimark bifurcation.

The remainder of the paper is organized as follows. In Section 2, local bifurcations of discrete-time system are summarized. In Section 3, a general model for PWM DC-DC converters developed by the authors in [1, 2] is recalled. In Section 4, necessary conditions for period-doubling bifurcation and saddle-node bifurcation in PWM DC-DC converters are obtained. Examples of the three bifurcations associated with instabilities in PWM DC-DC converters are given. Conclusions are collected in Section 5.

2 Local Bifurcations in Discrete-Time Systems

In this section, the basic bifurcation theory used in the paper is recalled. For details, the reader is referred to [36, 37, 38].

Consider a discrete-time parameter-dependent system

$$x_{n+1} = f(x_n, \alpha), \qquad x \in \mathbf{R}^N, \qquad \alpha \in \mathbf{R} \tag{1}$$

The parameter α is called the bifurcation parameter. Suppose $x = x_0(\alpha)$ is a fixed point of Eq. (1) for all α. Denote $A(\alpha) = f_x(x_0(\alpha), \alpha)$, the Jacobian of f with respect to x at $(x_0(\alpha), \alpha)$. The fixed point $x = x_0(\alpha)$ is called a *hyperbolic* fixed point if $A(\alpha)$ has no eigenvalues on the unit circle in the complex plane. If a bifurcation occurs, then it must occur for a value α_* of α for which $A(\alpha)$ is nonhyperbolic. There are three ways in which parameter variation can result in hyperbolicity being violated, and these are associated with three distinct bifurcations.

Three Local Bifurcations

1. Period-doubling bifurcation (the bifurcation associated with a real eigenvalue passing through the value -1): There is a curve of fixed point in the x-α plane on both sides of $\alpha = \alpha_*$ and a curve of period-two points on one side of $\alpha = \alpha_*$ intersecting with the first curve at $\alpha = \alpha_*$.
2. Saddle-node bifurcation (the bifurcation associated with a real eigenvalue reaching the value 1): There is a unique curve of fixed points in the x-α plane passing through $(x_0(\alpha), \alpha_*)$ and locally lying on one side of $\alpha = \alpha_*$.
3. Neimark bifurcation (the bifurcation associated with a complex-conjugate pair of eigenvalues crossing the unit circle): There is a curve of fixed points in the x-α plane on both sides of $\alpha = \alpha_*$ and the emergence of a small-amplitude "invariant circle" around the fixed-point on one side of $\alpha = \alpha_*$.

Other names for these bifurcations are sometimes used. The period-doubling bifurcation is also called flip bifurcation; the saddle-node bifurcation is also called fold bifurcation or tangent bifurcation; and the Neimark bifurcation is also called secondary Hopf bifurcation.

3 General Sampled-Data Model for PWM Converters

Without loss of generality, only continuous conduction mode [39, pp. 165-168] is considered. A summary of the sampled-data modeling of closed-loop PWM converters discussed in [1, 2] is given. This includes a general block diagram model as well as associated nonlinear and linearized sampled-data models. This model is applicable both to voltage mode control [39, pp. 322-336] and current mode control [39, pp. 337-340].

A block diagram model for a PWM converter in continuous conduction mode is shown in Fig. 1. In the diagram, $A_1, A_2 \in \mathbf{R}^{N\times N}$, $B_1, B_2 \in \mathbf{R}^{N\times 1}$, $C, E_1, E_2 \in \mathbf{R}^{1\times N}$, and $D \in \mathbf{R}$ are constant matrices, $x \in \mathbf{R}^N$, $y \in \mathbf{R}$ are the state and the feedback signal, respectively, and N is the state dimension, typically given by the number of energy storage elements in the converter. The source voltage is v_s, and the output voltage is v_o. The notation v_r denotes the reference signal, which could be a voltage or current reference. The reference signal v_r is allowed to be time-varying, although it is constant in most applications. The signal $h(t)$ is a T-periodic ramp. In current mode control, it is used to model a compensating ramp. The clock has the same frequency $f_s = 1/T$ as the ramp. This frequency is called the switching frequency. Within a clock period, the dynamics is switched between the two stages S_1 and S_2. The system is in S_1 immediatedly following a clock pulse, and switches to S_2 at instants when $y(t) = h(t)$.

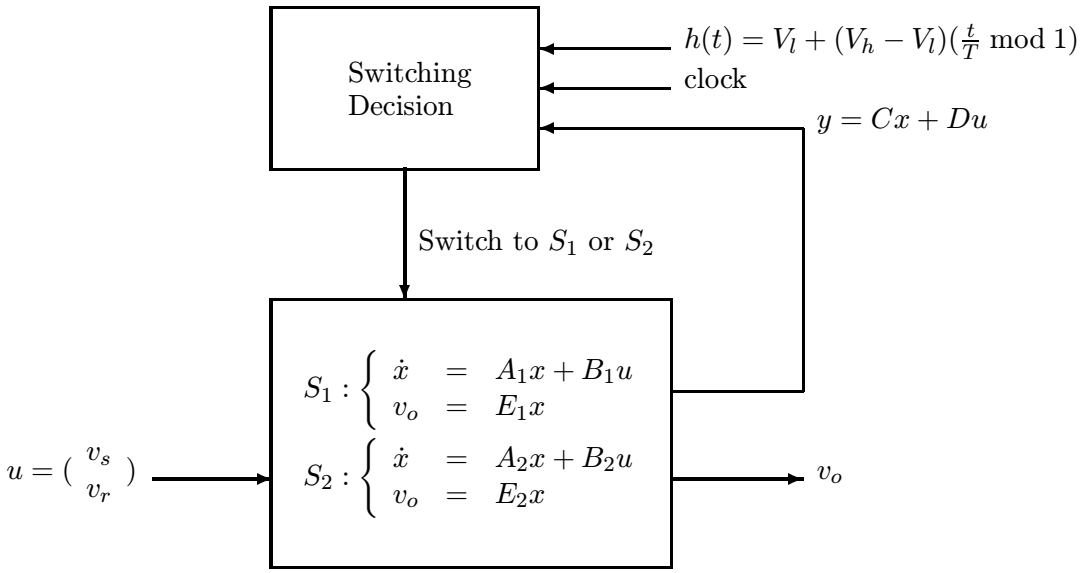

Figure 1: Block diagram model for PWM converter operation in continuous conduction mode

Consider the cycle $t \in [nT, (n+1)T)$. Take $u = (v_s, v_r)$ to be constant within the cycle, and denote its value by $u_n = [v_{sn}, v_{rn}]'$. Let $x_n = x(nT)$ and $v_{on} = v_o(nT)$. Denote by $nT + d_n$ the switching instant within the cycle when $y(t)$ and $h(t)$ intersect. Then, the system in Fig. 1 has the following sampled-data dynamics:

$$\begin{aligned} x_{n+1} &= f(x_n, u_n, d_n) \\ &= e^{A_2(T-d_n)}(e^{A_1 d_n}x_n + \int_0^{d_n} e^{A_1(d_n-\sigma)}d\sigma B_1 u_n) + \int_{d_n}^{T} e^{A_2(T-\sigma)}d\sigma B_2 u_n \qquad (2) \\ g(x_n, u_n, d_n) &= C(e^{A_1 d_n}x_n + \int_0^{d_n} e^{A_1(d_n-\sigma)}d\sigma B_1 u_n) + Du_n - h(d_n) \end{aligned}$$

$$= \quad 0 \tag{3}$$

An illustration of mapping from x_n to x_{n+1} is shown in Fig. 2.

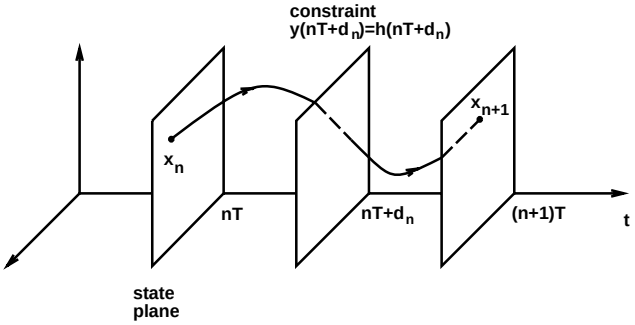

Figure 2: Illustration of sampled-data dynamics of PWM converter

A periodic solution $x^0(t)$ in Fig. 1 corresponds to a fixed point $x^0(0)$ in the sampled-data dynamics (2) and (3). Let the fixed point be $(x_n, u_n, d_n) = (x^0(0), u, d)$, where $u = [V_s, V_r]'$. Substituting this fixed point into Eq. (2) gives (assuming 1 is not an eigenvalue of $e^{A_2(T-d)}e^{A_1 d}$)

$$\begin{aligned} x^0(0) &= (I - e^{A_2(T-d)}e^{A_1 d})^{-1}(e^{A_2(T-d)}\int_0^d e^{A_1(d-\sigma)}d\sigma B_1 u \\ &\quad + \int_d^T e^{A_2(T-\sigma)}d\sigma B_2 u) \end{aligned} \tag{4}$$

Similarly, $x^0(d)$ can be expressed as a function of d,

$$\begin{aligned} x^0(d) &= (I - e^{A_1 d}e^{A_2(T-d)})^{-1}(e^{A_1 d}\int_d^T e^{A_2(T-\sigma)}d\sigma B_2 u \\ &\quad + \int_0^d e^{A_1(d-\sigma)}d\sigma B_1 u) \end{aligned} \tag{5}$$

From Eq. (3),

$$Cx^0(d) + Du - h(d) = 0 \tag{6}$$

which is a 1-dimensional equation in one unknown d and can be solved by Newton's method.

Using a hat $\hat{}$ to denote small perturbations (e.g., $\hat{x}_n = x_n - x^0(0)$), the system (2), (3) has the linearized dynamics

$$\hat{x}_{n+1} = \Phi\hat{x}_n + \Gamma\hat{u}_n = \Phi\hat{x}_n + \Gamma_1\hat{v}_{sn} + \Gamma_2\hat{v}_{rn} \tag{7}$$

where

$$\begin{aligned} \Phi &= e^{A_2(T-d)}(I - \frac{((A_1 - A_2)x^0(d) + (B_1 - B_2)u)C}{C(A_1 x^0(d) + B_1 u) - \dot{h}(d)})e^{A_1 d} \\ &= e^{A_2(T-d)}(I - \frac{(\dot{x}^0(d^-) - \dot{x}^0(d^+))C}{C\dot{x}^0(d^-) - \dot{h}(d)})e^{A_1 d} \end{aligned} \tag{8}$$

$$\Gamma = e^{A_2(T-d)}(\int_0^d e^{A_1\sigma}d\sigma B_1 - \frac{\dot{x}^0(d^-) - \dot{x}^0(d^+)}{C\dot{x}^0(d^-) - \dot{h}(d)}(C\int_0^d e^{A_1\sigma}d\sigma B_1 + D)) + \int_0^{T-d} e^{A_2\sigma}d\sigma B_2 \tag{9}$$

Here $\dot{x}^0(d^-)$ and $\dot{x}^0(d^+)$ denote the time derivative of $x^0(t)$ at $t = d^-$ and d^+, respectively. Local stability of the converter is determined by the eigenvalues of Φ, denoted as $\sigma[\Phi]$.

4 Bifurcations in PWM DC-DC Converters

This section contains the main results of the paper. First, general necessary conditions for period-doubling bifurcation and saddle-node bifurcation are obtained. This is followed by detailed illustrations of period-doubling, saddle-node and Neimark bifurcations for PWM DC-DC converters.

4.1 Necessary Conditions for Period-Doubling Bifurcation and Saddle-Node Bifurcation

The periodic solution $x^0(t)$ in the system of Fig. 1 is asymptotically *orbitally* stable [40, 1] if all of the eigenvalues of Φ are inside the unit circle of the complex plane. As a system parameter (bifurcation parameter) varies, the trajectory of the eigenvalues can be plotted. As the trajectory crosses the unit circle of the complex plane, a bifurcation occurs.

Two results are obtained. The first result gives a condition for λ to be an eigenvalue of Φ. This is then applied to check for the occurrence of period-doubling bifurcation and saddle-node bifurcation.

Theorem 1 *Suppose that λ is not an eigenvalue of $e^{A_2(T-d)}e^{A_1 d}$. Then λ is an eigenvalue of Φ if and only if*

$$1 + Ce^{A_1 d}(\lambda I - e^{A_2(T-d)}e^{A_1 d})^{-1}e^{A_2(T-d)}\frac{\dot{x}^0(d^-) - \dot{x}^0(d^+)}{C\dot{x}^0(d^-) - \dot{h}(d)} = 0 \tag{10}$$

Proof: Suppose λ is not an eigenvalue of $e^{A_2(T-d)}e^{A_1 d}$, then

$$\begin{aligned}
\det[\lambda I - \Phi] &= \det[\lambda I - e^{A_2(T-d)}e^{A_1 d}] \cdot \\
&\quad \det[I + (\lambda I - e^{A_2(T-d)}e^{A_1 d})^{-1}e^{A_2(T-d)}\frac{\dot{x}^0(d^-) - \dot{x}^0(d^+)}{C\dot{x}^0(d^-) - \dot{h}(d)}Ce^{A_1 d}] \\
&= \det[\lambda I - e^{A_2(T-d)}e^{A_1 d}] \cdot \\
&\quad (1 + Ce^{A_1 d}(\lambda I - e^{A_2(T-d)}e^{A_1 d})^{-1}e^{A_2(T-d)}\frac{\dot{x}^0(d^-) - \dot{x}^0(d^+)}{C\dot{x}^0(d^-) - \dot{h}(d)})
\end{aligned}$$

So λ is an eigenvalue of Φ if and only if

$$1 + Ce^{A_1 d}(\lambda I - e^{A_2(T-d)}e^{A_1 d})^{-1}e^{A_2(T-d)}\frac{\dot{x}^0(d^-) - \dot{x}^0(d^+)}{C\dot{x}^0(d^-) - \dot{h}(d)} = 0$$

□

Corollary 1
(i) If the system parameters correspond to an occurrence of period-doubling bifurcation ($\lambda = -1$), then

$$1 + Ce^{A_1 d}(-I - e^{A_2(T-d)}e^{A_1 d})^{-1}e^{A_2(T-d)}\frac{\dot{x}^0(d^-) - \dot{x}^0(d^+)}{C\dot{x}^0(d^-) - \dot{h}(d)} = 0 \tag{11}$$

(ii) If the system parameters correspond to an occurrence of saddle-node bifurcation ($\lambda = 1$), then

$$1 + Ce^{A_1 d}(I - e^{A_2(T-d)}e^{A_1 d})^{-1}e^{A_2(T-d)}\frac{\dot{x}^0(d^-) - \dot{x}^0(d^+)}{C\dot{x}^0(d^-) - \dot{h}(d)} = 0 \tag{12}$$

In the PWM DC-DC converter, instabilities involve bifurcations of the periodic solution. The three local bifurcations are described in more detail next.

In the period-doubling bifurcation, a $2T$-periodic solution arises besides the original T-periodic solution. In most PWM DC-DC converters, the period-doubling bifurcation is supercritical, where the $2T$-periodic solution is stable and the original T-periodic solution becomes unstable. An illustration of such a bifurcation is shown in Fig. 3.

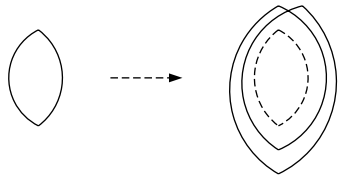

Figure 3: Periodic solution before and after supercritical period-doubling bifurcation (solid line for stable solution and dashed line for unstable solution)

In the saddle-node bifurcation, a stable T-periodic solution collides with an unstable one at the bifurcation point, and no periodic solution exists after the bifurcation. This may explain some jump phenomena, or sudden disappearance of the nominal periodic solution in DC-DC converters. An illustration of such a bifurcation is shown in Fig. 4.

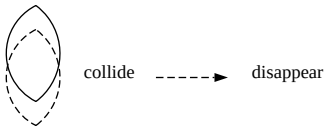

Figure 4: Periodic solution before and after saddle-node bifurcation (solid line for stable solution and dashed line for unstable solution)

An illustration of a (supercritical) Neimark bifurcation is given in Fig. 5. After the bifurcation, the steady-state trajectory is on a torus (with the time axis circled as another dimension). The two angular frequency vectors (ω_s and ω_f) of the trajectory in the figure are perpendicular to each other. One of them is the same as the angular switching frequency $\omega_s = 2\pi f_s$. Another one can be determined from the bifurcation point where the eigenvalue trajectory of Φ crosses the unit circle of the complex plane. Its value is $f_s \cdot \angle\sigma(\Phi)$, f_s times the argument (i.e., phase) of the pair of eigenvalue of Φ crossing the unit circle. The state trajectory will be periodic (phase-locking) if these two frequencies are commensurate; otherwise it will be quasiperiodic.

4.2 Period-Doubling Bifurcation in Buck Converter under Voltage Mode Control

Consider the example [6] of a buck converter under voltage mode control shown in Fig. 6. Let $T = 400\mu s$, $L = 20mH$, $C = 47\mu F$, $R = 22\Omega$, $V_r = 11.3V$, $g_1 = 8.4$, $V_l = 3.8V$, $V_h = 8.2V$, (then $h(t) = 3.8 + 4.4[\frac{t}{T} \bmod 1]$), and let V_s be the bifurcation parameter.

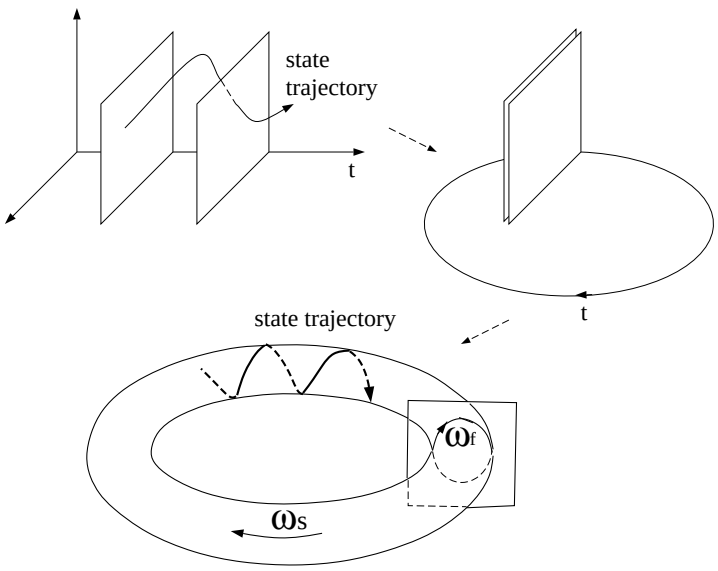

Figure 5: State trajectory after Neimark bifurcation

Let the state be $x = (i_L, v_C)$. In terms of the block diagram model in Fig. 1, one has

$$\begin{aligned} A_1 &= A_2 = \begin{bmatrix} 0 & \frac{-1}{L} \\ \frac{1}{C} & \frac{-1}{RC} \end{bmatrix} \\ B_1 &= \begin{bmatrix} 0 \\ 0 \end{bmatrix} \qquad\qquad B_2 = \begin{bmatrix} \frac{1}{L} \\ 0 \end{bmatrix} \\ C &= \begin{bmatrix} 0 & g_1 \end{bmatrix} \qquad\qquad D = \begin{bmatrix} 0 & -g_1 \end{bmatrix} \\ E_1 &= E_2 = \begin{bmatrix} 0 & 1 \end{bmatrix} \end{aligned}$$

The bifurcation diagram obtained from simulations is shown in Fig. 7. The circuit undergoes a series of period-doubling bifurcations beginning at $V_s = 24.5V$ approximately. The eigenvalues of Φ (i.e. $\sigma(\Phi)$) as V_s varies from 13.1 to $25.068V$ is shown in Fig. 8. They are calculated from Eq. (8), while [19] obtains the same graph by numerical estimation. One eigenvalue of Φ is -1 when $V_s = 24.527$, which agrees exactly with the numerical results in Fig. 7.

Another way to determine the period-doubling bifurcation point is discussed next. From Eqs. (5) and (6), the following equation relating V_s and d is obtained:

$$V_s = \frac{h(d) + g_1 V_r}{C e^{A_2 d}(I - e^{A_2 T})^{-1} A_2^{-1}(e^{A_2(T-d)} - I)B_2} \tag{13}$$

From Eqs. (11) and (5), another equation relating V_s and d at the period-doubling bifurcation is obtained:

$$V_s = \frac{\dot{h}(d)}{C[(I + e^{-A_2 T})^{-1} + (I - e^{A_2 T})^{-1}(e^{A_2 T} - e^{A_2 d})]B_2} \tag{14}$$

The loci of these two equations are shown in Fig. 9. From the figure, the period-doubling bifurcation point can be determined. The critical value of source voltage is $V_{s,*} = 24.527V$ (at $d_* = 2.039 \times 10^{-4}$). This agrees with the result using the sampled-data approach.

After period-doubling bifurcation, the original periodic solution becomes unstable, and a stable $2T$-periodic solution arises. Take $V_s = 26V$, for example. Performing steady-state analysis stated in [1, 2], the unstable T-periodic solution and the stable $2T$-periodic solution can be obtained. They are shown as the dashed line and solid line respectively in Fig. 10.

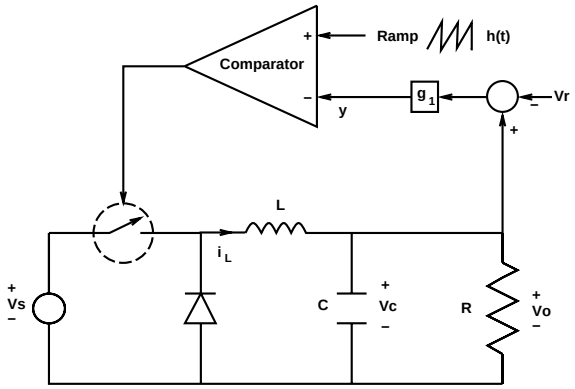

Figure 6: System diagram

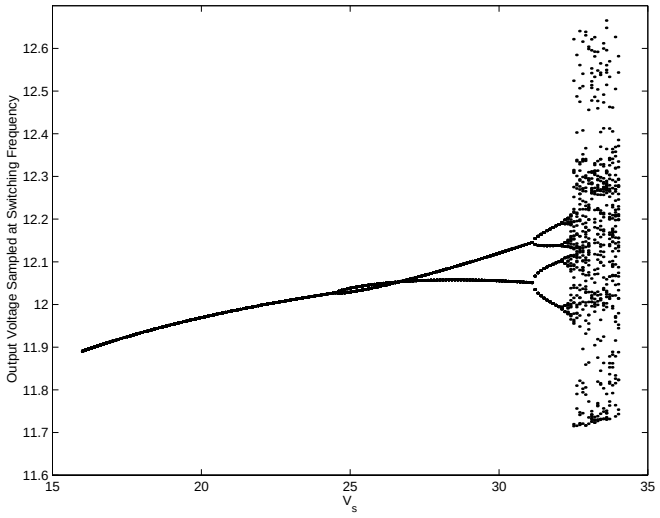

Figure 7: Bifurcation diagram of the circuit in Fig. 6. Unstable periodic solutions (e.g., $2T$-periodic solutions) are not plotted.

4.3 Period-Doubling Bifurcation in Boost Converter under Current Mode Control

Consider the example [16] of a boost converter under current mode control shown in Fig. 11, where $T = 100\mu s$, $V_s = 10V$, $L = 1mH$, $C = 12\mu F$, $R = 20\Omega$, and V_r (current reference) is taken to be the bifurcation parameter.

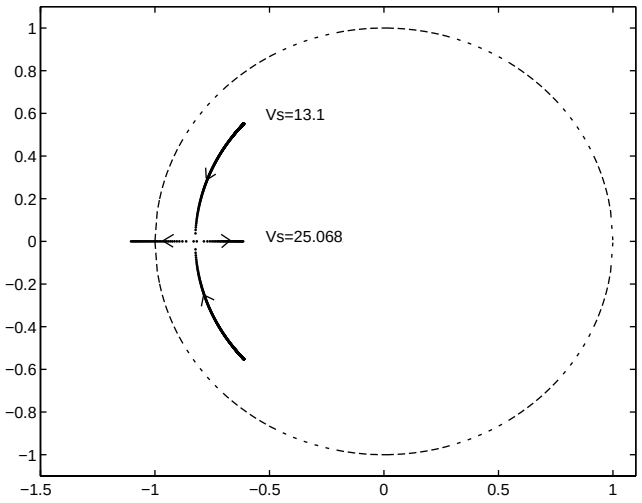

Figure 8: $\sigma(\Phi)$ as V_s varies from 13.1 to 25.068

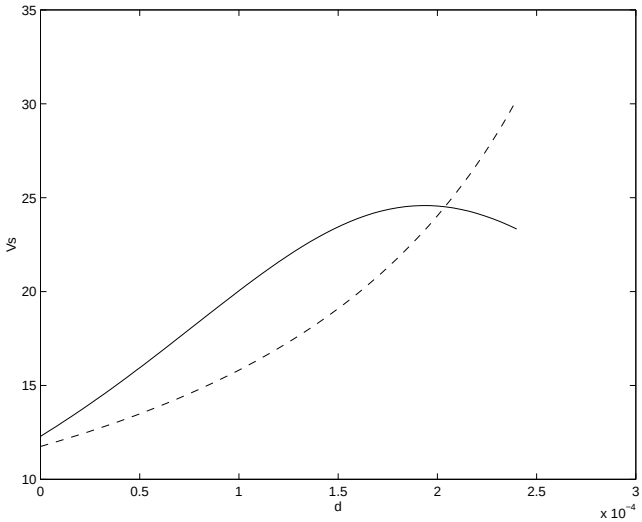

Figure 9: Plot of Eq. (13) (dashed line) and Eq. (14) (solid line). The intersection $(d, V_s) = (0.0002039, 24.527)$ is the period-doubling bifurcation point

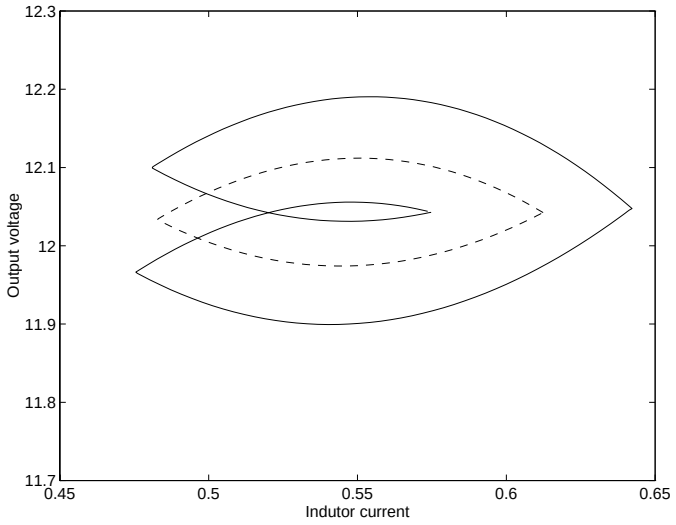

Figure 10: Unstable T-periodic solution (dashed line) and stable $2T$-periodic solution (solid line) for $V_s = 26V$

Let the state be $x = (i_L, v_C)$. In terms of the block diagram model in Fig. 1, one has

$$\begin{aligned} A_1 &= \begin{bmatrix} 0 & 0 \\ 0 & \frac{-1}{RC} \end{bmatrix} & A_2 &= \begin{bmatrix} 0 & \frac{-1}{L} \\ \frac{1}{C} & \frac{-1}{RC} \end{bmatrix} \\ B_1 &= B_2 = \begin{bmatrix} \frac{1}{L} \\ 0 \end{bmatrix} \\ C &= \begin{bmatrix} 1 & 0 \end{bmatrix} & D &= \begin{bmatrix} 0 & -1 \end{bmatrix} \\ E_1 &= E_2 = \begin{bmatrix} 0 & 1 \end{bmatrix} & h(t) &= 0 \end{aligned}$$

The bifurcation diagram of the circuit is shown in Fig. 12, where a period-doubling bifurcation occurs at around $V_r = 1.7$.

The loci of $\sigma(\Phi)$ as V_r varies from 0.6634 to 3.3759 is shown in Fig. 13. One eigenvalue of Φ is -1 when $V_r = 1.7457$ (and $D_c = 0.433$), which agrees exactly with the simulation result in [16].

4.4 Saddle-Node Bifurcation in Buck Converter under Discrete-Time Control

Take the *power stage* in Section 4.2. Change V_s to $20V$ and add a discrete-time controller. The resulting system diagram is shown in Fig. 14. The switching decision in the $(n+1)$-st cycle, $t \in [nT, (n+1)T)$, is as follows (similar to a leading-edge modulation): the switch is turned off at $t = nT$ and turned on at $t = nT + d_n$. The switching instant d_n is updated by $d_n = \ell(0.3T - k_i(i_n - I_p) - k_v(v_n - V_p))$, where $k_i = -8.574 \times 10^{-4}$, $k_v = 5.53 \times 10^{-5}$, $I_p = 0.6785$, $V_p = 14.0263$, and ℓ is a limiter:

$$\ell(t) = \begin{cases} 0 & \text{for } t \le 0 \\ t & \text{for } t \in (0, T] \\ T & \text{for } t > T \end{cases} \tag{15}$$

The discrete-time law above is very interesting. It will produce different static and periodic solutions for different V_s. First, it can be shown that the switch being always on is a possible

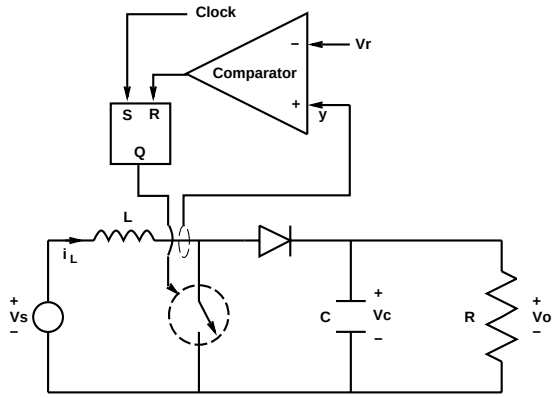

Figure 11: System diagram for the circuit in Section 4.3

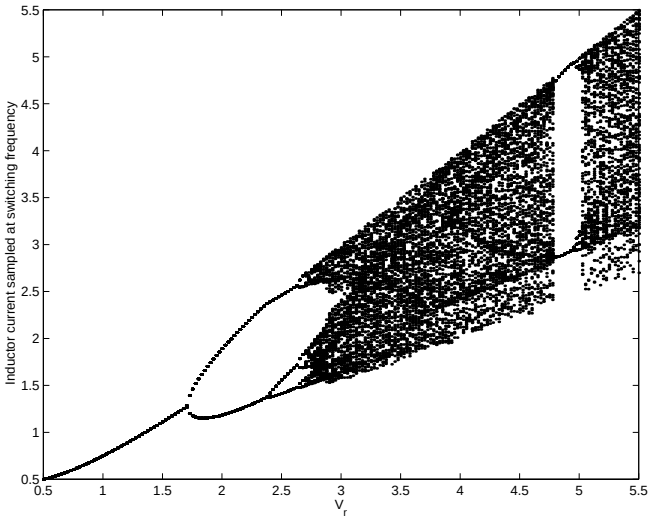

Figure 12: Bifurcation diagram of the circuit in Fig. 11

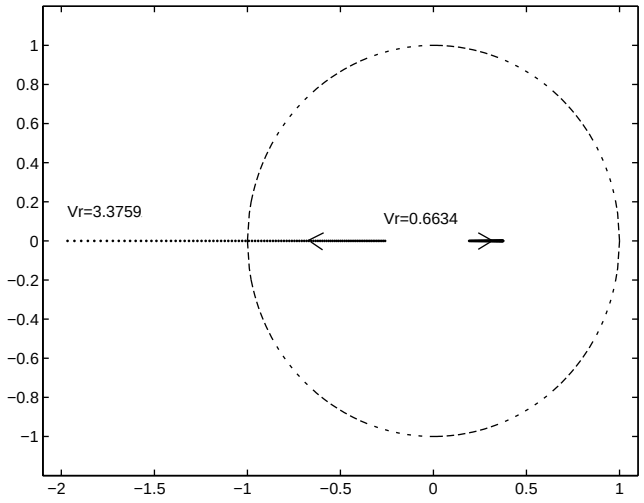

Figure 13: $\sigma(\Phi)$ as V_r varies from 0.6634 to 3.3759

operation under some circumstances. In such an operation, $d_n = 0$ for any n. Also when the switch is always on, $v_o = V_s$, $i = V_s/R$, (both are constant instead of being periodic,) and therefore $v_n = V_s$, $i_n = V_s/R$. From Eq. (15), the following inequality needs to hold in order to make $d_n = 0$:

$$\begin{aligned} 0.3T - k_i(i_n - I_p) - k_v(v_n - V_p) &= 0.3T - k_i(\frac{V_s}{R} - I_p) - k_v(V_s - V_p) \\ &= 0.3T + k_i I_p + k_v V_p - (\frac{k_i}{R} + k_v)V_s \\ &\leq 0 \end{aligned}$$

Therefore for $V_s > (\frac{k_i}{R} + k_v)/(0.3T + k_i I_p + k_v V_p) = 19.213$, the switch can be always on.

However, the switch being always on is not the only possible operation for $V_s > 19.213$. It can be shown that for $V_s \in (19.213, 20)$, there are another two periodic solutions: one is stable, another one is unstable.

Take $V_s = 19.9$, for example. Performing steady-state analysis stated in [1, 2], one stable periodic solution with duty cycle 0.6267 and one unstable periodic solution with duty cycle 0.7878 can be obtained. They are shown as the solid line and dashed line respectively in Fig. 15. The stable one has output voltage around $12.5V$; unstable one has output voltage around $15.7V$. As V_s is further increased, these two periodic solutions become closer and collide when $V_s = 20$. For $V_s = 20$, one eigenvalue of Φ is 1 and a saddle-node bifurcation occurs. If V_s is increased a little bit above 20, the operation suddenly jumps to the situation where the switch is always on and the output voltage jumps from $14V$ to $20V$.

The circuit is simulated for $V_s \in [18.5, 20.5]$ and the resulting bifurcation diagram is shown Fig. 16. In the figure, the upper solid line is for the operation when the switch is always on (duty cylcle=1), and the dashed line and the lower solid line are for unstable and stable periodic solutions respectively with duty cycle less than 1. For V_s below 19.213, there is only one stable periodic solution and the output voltage is regulated below $11V$.

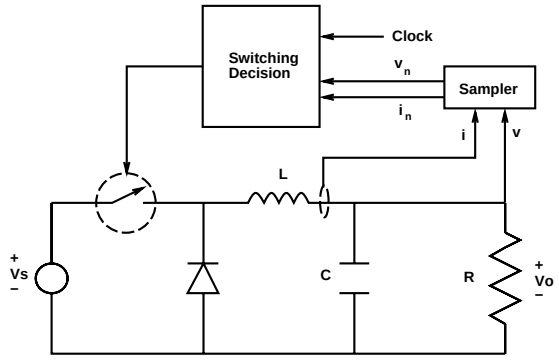

Figure 14: System diagram for the circuit in Section 4.4

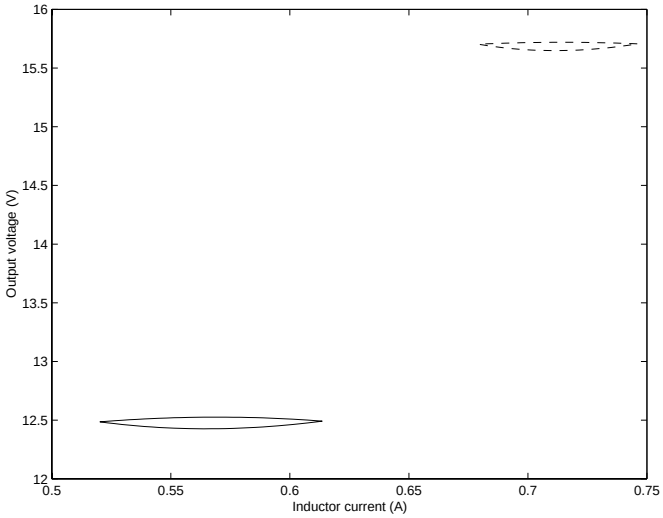

Figure 15: Stable periodic solution (solid line) and unstable periodic solution (dashed line) for $V_s = 19.9V$

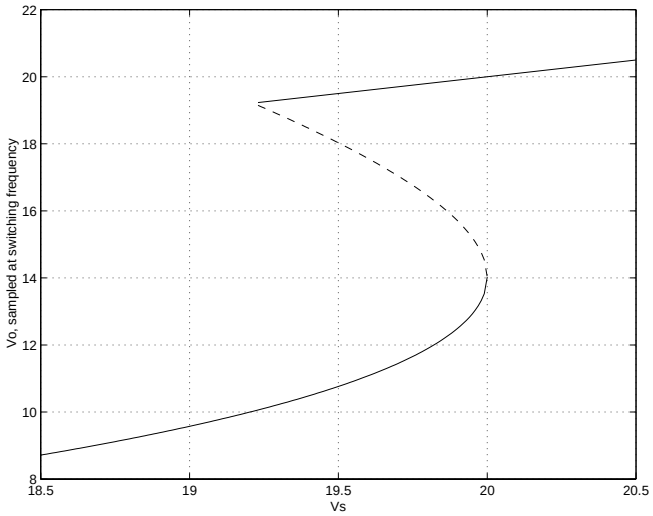

Figure 16: Bifurcation diagram of the buck converter in Section 4.4. Solid lines indicate stable solutions and the dashed line indicates an unstable solution

4.5 Neimark Bifurcation in Buck Converter under Voltage Mode Control

Consider the example [41, p.228] of a buck converter under voltage mode control shown in Fig. 17. Let $f_s = 15kHz$, $L = 0.9mH$, $C = 22\mu F$, $R = 20\Omega$, $V_r = 10V$, $R_1 = R_2 = 7.5k\Omega$, $R_3 = 60k\Omega$, $C_2 = 0.4\mu F$, $V_l = 2.8V$, $V_h = 8.2V$, (then $h(t) = 2.8 + 5.4[\frac{t}{T} \bmod 1]$). All parasitic resistances are ignored.

Let the state $x = (i_L, v_C, v_{c2})$, In terms of the representation in Fig. 1, one has

$$
\begin{array}{rclcrcl}
A_1 & = & A_2 = \begin{bmatrix} 0 & \frac{-1}{L} & 0 \\ \frac{1}{C} & \frac{-1}{RC} & 0 \\ 0 & \frac{1}{R_1C_2} & \frac{-1}{R_3C_2} \end{bmatrix} & & & & \\
B_1 & = & \begin{bmatrix} \frac{1}{L} & 0 \\ 0 & 0 \\ 0 & \frac{-1}{C_2}(\frac{1}{R_1}+\frac{1}{R_2}) \end{bmatrix} & & B_2 & = & \begin{bmatrix} 0 & 0 \\ 0 & 0 \\ 0 & \frac{-1}{C_2}(\frac{1}{R_1}+\frac{1}{R_2}) \end{bmatrix} \\
C & = & \begin{bmatrix} 0 & 0 & -1 \end{bmatrix} & & D & = & \begin{bmatrix} 0 & 1 \end{bmatrix} \\
E_1 & = & E_2 = \begin{bmatrix} 0 & 1 & 0 \end{bmatrix} & & & &
\end{array}
$$

Solving Eqs. (6) and(4) gives $x^0(0) = (0.7798, 20.4825, 3.5214)$, which has output voltage around $20V$. This result is quite different from [41], which has output voltage around $10V$.

After examing the system, the reference voltage V_r should be changed to $5V$, instead of $10V$ in [41], to have output voltage around $10V$. In the following, $V_r = 5V$ is used.

Solving Eqs. (6) and(4) again gives $x^0(0) = (0.2539, 10.0053, 0.3918))$, which now has output voltage around $10V$ as expected. The eigenvalues of Φ are 0.8799 and $0.8797 \pm 0.4474i$, which are inside the unit circle. Thus the system is asymptotically orbitally stable.

As V_s is increased from $30V$, the magnitude of the complex pair of eigenvalues begin to grow. For $V_s = 36.9V$, the eigenvalues $(0.8897 \pm 0.4567i)$ exit the unit circle. Thus a Neimark bifurcation occurs. Besides oscillating at frequency f_s, another oscillating frequency $\frac{f_s}{2\pi}\angle(0.8897 + 0.4567i) =$

$1132Hz$ is expected. Since these two frequencies are not commensurate, the steady state is quasiperiodic.

As in [41], the circuit with $V_s = 30V$ and $V_s = 50V$ are simulated. State space trajectories and output voltage waveforms are used to explain the dynamics associated with the Neimark bifurcation. More detailed explanations than [41] are given as follows. For $V_s = 30V$, the stable periodic solution $x^0(t)$ can be obtained through a steady-state analysis discussed in [1, 2]. It is shown as a solid line in Fig. 18. As V_s reaches $36.9V$, the Neimark bifurcation occurs. The stable periodic solution becomes unstable. For $V_s = 50V$, this unstable periodic solution can be obtained similarly and it is shown as a dashed line in Fig. 18. A quasiperiodic state trajectory arises after the Neimark bifurcation occurs. It is shown in Fig. 19 for $V_s = 50V$.

Output voltage waveforms of the quasiperiodic steady state and the unstable periodic solution are shown as solid line (with larger amplitude) and dashed line respectively in Fig. 20 for $V_s = 50V$. From the figure, the quasiperiodic steady state has two oscillating frequencies as expected: f_s modulated by a lower frequency around $1132Hz$.

In [41], the circuit is simulated without mention of the Neimark bifurcation, the quasiperiodic steady state or the unstable periodic solution.

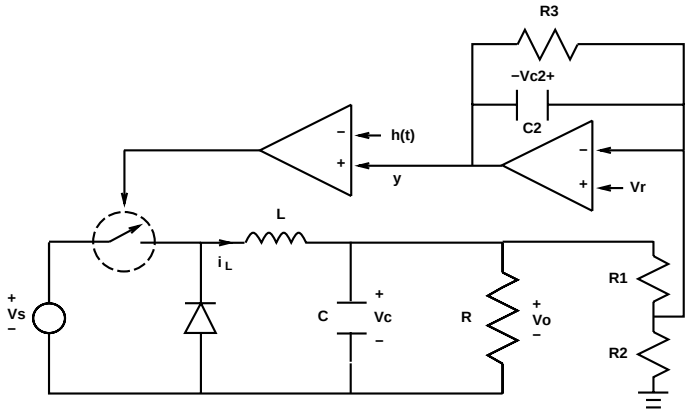

Figure 17: System diagram for the circuit in Section 4.5

4.6 Neimark Bifurcation in Buck Converter with Input Filter under Voltage Mode Control

An input filter is added to the circuit in Section 4.2 with $V_s = 15.8V$. The resulting system diagram is shown in Fig. 21. The input filter parameters are $L_f = 2.5mH$, $C_f = 160\mu F$, and R_p is added to adjust the damping. The angular resonance frequency of input filter is $\omega_r = \frac{1}{\sqrt{L_f C_f}} = 1581.1$.

Let the state be $x = (i_L, v_C, i_f, v_f)$, where i_f and v_f are the inductor current and capacitor

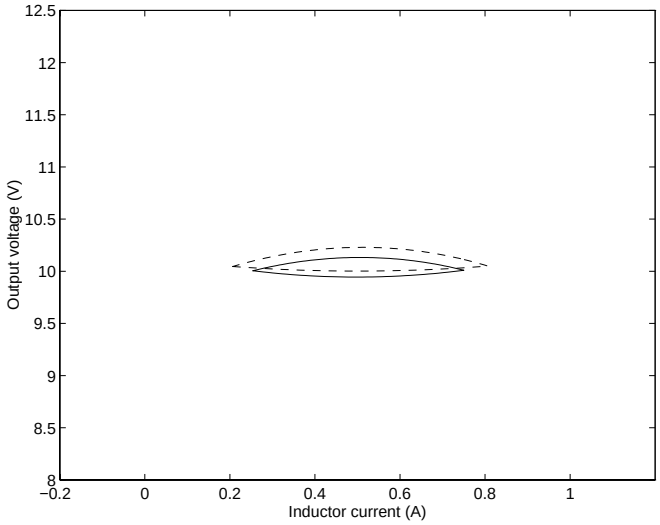

Figure 18: Stable periodic solution (solid line) for $V_s = 30V$ becomes unstable periodic solution (dashed line) for $V_s = 50V$

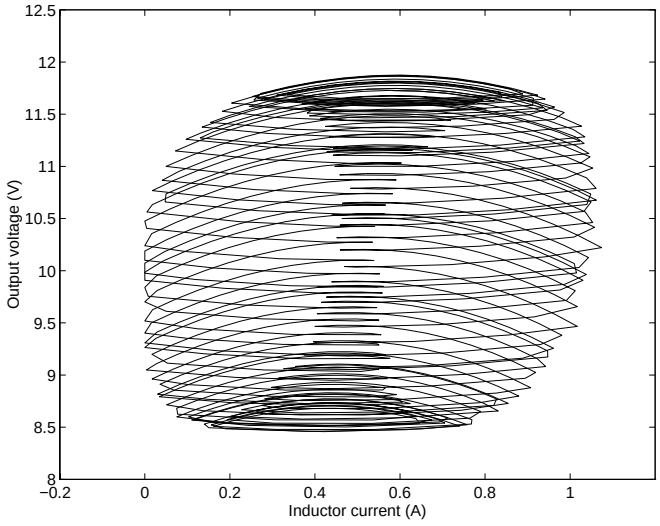

Figure 19: Quasiperiodic state trajectory in state space for $V_s = 50V$

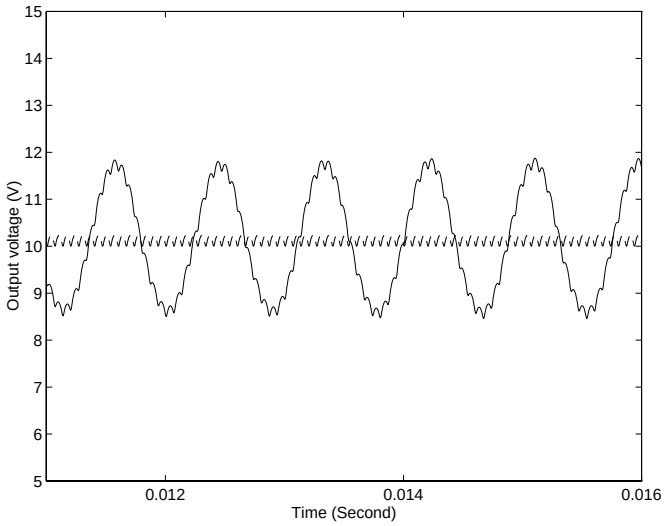

Figure 20: Quasiperiodic output voltage (solid line with larger amplitude) and unstable (also unobserved) periodic output voltage (dashed line), both for $V_s = 50V$

voltage in the input filter respectively. In terms of the block diagram model in Fig. 1, one has

$$A_1 = \begin{bmatrix} 0 & \frac{-1}{L} & 0 & 0 \\ \frac{1}{C} & \frac{-1}{RC} & 0 & 0 \\ 0 & 0 & 0 & \frac{-1}{L_f} \\ 0 & 0 & \frac{1}{C_f} & \frac{-1}{R_pC_f} \end{bmatrix} \qquad A_2 = \begin{bmatrix} 0 & \frac{-1}{L} & 0 & \frac{1}{L} \\ \frac{1}{C} & \frac{-1}{RC} & 0 & 0 \\ 0 & 0 & 0 & \frac{-1}{L_f} \\ \frac{-1}{C_f} & 0 & \frac{1}{C_f} & \frac{-1}{R_pC_f} \end{bmatrix}$$

$$B_1 = B_2 = \begin{bmatrix} 0 \\ 0 \\ \frac{1}{L_f} \\ \frac{1}{R_pC_f} \end{bmatrix}$$

$$C = \begin{bmatrix} 0 & g_1 & 0 & 0 \end{bmatrix} \qquad D = \begin{bmatrix} 0 & -g_1 \end{bmatrix}$$

$$E_1 = E_2 = \begin{bmatrix} 0 & 1 & 0 & 0 \end{bmatrix}$$

The loci of $\sigma(\Phi)$ as R_p varies is shown in Fig. 22. One pair of eigenvalues are almost fixed at $-0.5963 \pm 0.5301i$, while the other pair moves as R_p varies. A Neimark bifurcation occurs when $R_p = 38.85$, where a pair of eigenvalues $0.8087 \pm 0.5883i$ crosses the unit circle. After the bifurcation, another oscillating angular frequency $f_s[\angle(0.81 + 0.59i)]$ is expected ($\angle$ denotes the angle in radian). This angular frequency has the same value as ω_r, which means that after the Neimark bifurcation the original oscillating frequency (i.e., the switching frequency $\omega_s = 2\pi f_s$) is modulated by the resonance frequency of input filter (ω_r). Since these two frequencies are not commensurate, the state trajectory is quasiperiodic.

4.7 Neimark Bifurcation in Buck Converter with Input Filter under Current Mode Control

The system diagram [42, p.96] is shown in Fig. 23, where $f_s = 30kHz$, $V_s = 15V$, $R = 10.4\Omega$, $L = 0.48mH$, $C = 30\mu F$, $R_L = 0.6\Omega$, with input filter parameters $R_{L1} = 0.25\Omega$, $L_f = 0.43mH$ and $C_f = 10.4\mu F$.

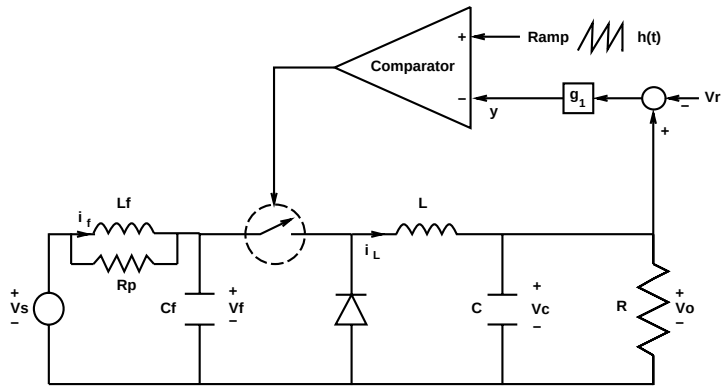

Figure 21: System diagram for the circuit in Section 4.6

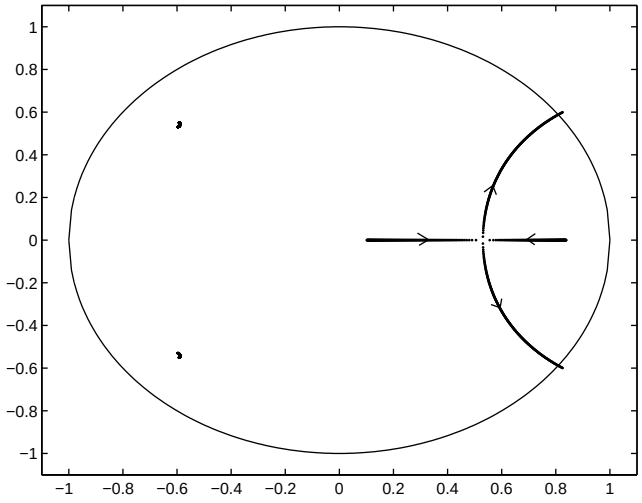

Figure 22: $\sigma(\Phi)$ as R_p varies from 1 to 100

Let the state be $x = (i_L, v_C, i_f, v_f)$, where i_f and v_f are the inductor current and capacitor voltage in the input filter, respectively. In terms of the block diagram model in Fig. 1, one has

$$A_1 = \begin{bmatrix} \frac{-R_L}{L} & \frac{-1}{L} & 0 & \frac{1}{L} \\ \frac{1}{C} & \frac{-1}{RC} & 0 & 0 \\ 0 & 0 & \frac{-R_{L1}}{L_f} & \frac{-1}{L_f} \\ \frac{-1}{C_f} & 0 & \frac{1}{C_f} & 0 \end{bmatrix} \qquad A_2 = \begin{bmatrix} \frac{-R_L}{L} & \frac{-1}{L} & 0 & 0 \\ \frac{1}{C} & \frac{-1}{RC} & 0 & 0 \\ 0 & 0 & \frac{-R_{L1}}{L_f} & \frac{-1}{L_f} \\ 0 & 0 & \frac{1}{C_f} & 0 \end{bmatrix}$$

$$B_1 = B_2 = \begin{bmatrix} 0 \\ 0 \\ \frac{1}{L_f} \\ 0 \end{bmatrix}$$

$$C = \begin{bmatrix} 1 & 0 & 0 & 0 \end{bmatrix} \qquad D = \begin{bmatrix} 0 & -1 \end{bmatrix}$$

$$E_1 = E_2 = \begin{bmatrix} 0 & 1 & 0 & 0 \end{bmatrix} \qquad h(t) = 0$$

The loci of $\sigma(\Phi)$ as the duty cycle D_c varies is shown in Fig. 24. An eigenvalue pair departs the unit circle for the parameter value $D_c = 0.2443$. In contrast, in reference [42] the circuit is said to become unstable when $D_c > 0.3$. Again as in the previous example, the bifurcated solution is on a torus, with angular frequencies, ω_s and $1/\sqrt{L_f C_f}$. As in Section 4.6, the frequency $1/\sqrt{L_f C_f}$ can be obtained numerically from the eigenvalue locus diagram in Fig. 24.

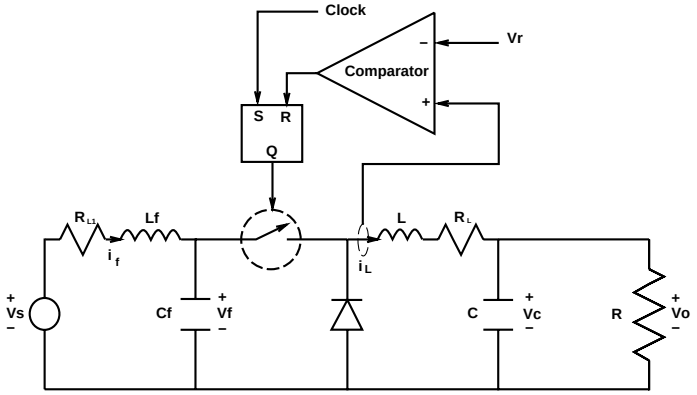

Figure 23: System diagram for Section 4.7

5 Concluding Remarks

Local bifurcations in PWM DC-DC converters were studied using nonlinear sampled-data models. The bifurcations considered were period-doubling bifurcation, saddle-node bifurcation, and Neimark bifurcation. Necessary conditions for period-doubling bifurcation and saddle-node bifurcation in PWM DC-DC converters are obtained. Instabilities in PWM DC-DC converters can be related to these bifurcations. In particular, input filter instability was shown to be related to the Neimark bifurcation.

Acknowledgments

This research has been supported in part by the the Office of Naval Research under Multidisciplinary University Research Initiative (MURI) Grant N00014-96-1-1123, and by the U.S. Air Force Office of Scientific Research under Grant F49620-96-1-0161.

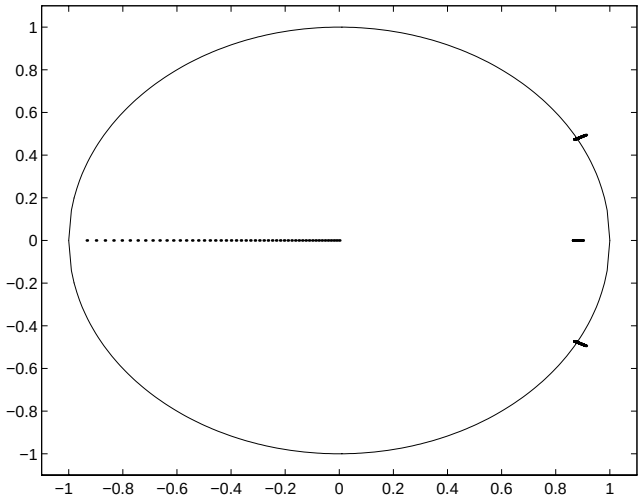

Figure 24: $\sigma(\Phi)$ as duty cycle D_c varies from 0 to 0.5, where the eigenvalue trajectories goes outward

References

[1] C.-C. Fang and E.H. Abed, "Sampled-data modeling and analysis of closed-loop PWM DC-DC converters," to appear at *IEEE International Symposium on Circuits and System*, May 1999.

[2] C.-C. Fang and E.H. Abed, "Sampled-data modeling and analysis of PWM DC-DC converters I. Closed-loop circuits," Tech. Rep. 98-54, Institute for Systems Research, University of Maryland, College Park, 1998, available at http://www.isr.umd.edu/TechReports/ISR/1998/.

[3] C Deisch, "Simple switching control method changes power converter into a current source," in *IEEE Power Electronics Specialists Conference Record*, 1978, pp. 300–306.

[4] A.R. Brown and R.D. Middlebrook, "Sampled-data modelling of switching regulators," in *IEEE Power Electronics Specialists Conference Record*, 1981, pp. 349–369.

[5] F.C.Y. Lee, R.P. Iwens, Yuan Yu, and J.E. Triner, "Generalized computer-aided discrete time-domain modeling and analysis of DC-DC converters," *IEEE Transactions on Industrial Electronics and Control Instrumentation*, vol. IECI-26, no. 2, pp. 58–69, 1979.

[6] D.C. Hamill, J.H.B. Deane, and J. Jefferies, "Modeling of chaotic DC-DC converters by iterated nonlinear mappings," *IEEE Transactions on Power Electronics*, vol. 7, no. 1, pp. 25–36, 1992.

[7] C.K. Tse, "Flip bifurcation and chaos in three-state boost switching regulators," *IEEE Transactions on Circuits and Systems-I: Fundamental Theory and Applications*, vol. 41, no. 1, pp. 16–23, 1994.

[8] K. Chakrabarty, G. Podder, and S. Banerjee, "Bifurcation behaviour of buck converter," *IEEE Transactions on Power Electronics*, vol. 11, no. 3, pp. 439–447, May 1995.

[9] S. Pavljasevic and D. Maksimovic, "Subharmonic oscillations in converters with current-mode programming under large parameter variations," in *IEEE Power Electronics Specialists Conference Record*, 1997, pp. 1323–1329.

[10] W.-H. Ki, "Analysis of subharmonic oscillation of fixed-frequency current- programming switch mode power converters," *IEEE Transactions on Circuits and Systems-I: Fundamental Theory and Applications*, vol. 45, no. 1, pp. 104–108, 1998.

[11] S.Y. Erich and W.M. Polivka, "Input filter filter design criteria for current-programmed regulators," *IEEE Transactions on Power Electronics*, vol. 7, no. 1, pp. 143–151, 1992.

[12] C.R. Kohut, "Input filter design criteria for switching regulators using current mode control," *IEEE Transactions on Power Electronics*, vol. 7, no. 3, pp. 469–479, 1992.

[13] Y. Jang and R.E. Erickson, "Physical origins of input filter oscillations in current programmed converters," *IEEE Transactions on Power Electronics*, vol. 7, no. 4, pp. 725–733, 1992.

[14] J.R. Wood, "Chaos: a real phenomenon in power electronics," in *Fourth Applied Power and Electronics Conference and Exposition*, 1989, pp. 115–124.

[15] J.H.B. Deane and D.C. Hamill, "Instability, subharmonics, and chaos in power electronics circuits," *IEEE Transactions on Power Electronics*, vol. 5, no. 3, pp. 260–268, 1990.

[16] J.H.B. Deane, "Chaos in a current-mode controlled boost DC-DC converter," *IEEE Transactions on Circuits and Systems-I: Fundamental Theory and Applications*, vol. 39, no. 8, pp. 680–683, 1992.

[17] I. Zafrany and S. Ben-Yaakov, "A chaos model of subharmonic oscillations in current mode PWM boost converters," in *IEEE Power Electronics Specialists Conference Record*, 1995, pp. 1111–1117.

[18] J.L.R. Marrero, J.M. Font, and G.C. Verghese, "Analysis of the chaotic regime for DC-DC converters under current-mode control," in *IEEE Power Electronics Specialists Conference Record*, 1996, pp. 1477–1483.

[19] E. Fossas and G. Olivar, "Study of chaos in the buck converter," *IEEE Transactions on Circuits and Systems-I: Fundamental Theory and Applications*, vol. 43, no. 1, pp. 13–25, 1996.

[20] F.D. Tan and R.S. Ramshaw, "Instabilities of a boost converter system under large parameter variations," *IEEE Transactions on Power Electronics*, vol. 4, no. 4, pp. 397–408, 1989.

[21] P.T. Krein and R.M. Bass, "Types of instability encountered in simple power electronic circuits: unboundedness, chattering, and chaos," in *Fifth Annual Applied Power Electronics Conference and Exposition*, 1990, pp. 191–194.

[22] S. Pavljasevic and D. Maksimovic, "Using a discrete-time model for large-signal analysis of a current-programmed boost converter," in *IEEE Power Electronics Specialists Conference Record*, 1991, pp. 715–721.

[23] M. di Bernardo, F. Garofalo, L Glielmo, and F. Vasca, "Quasi-periodic behaviors in DC/DC converters," in *IEEE Power Electronics Specialists Conference Record*, 1996, pp. 1376–1381.

[24] W.C.Y. Chan and C.K. Tse, "Study of bifurcations in current-programmed DC/DC boost converters: from quasiperiodicity to period-doubling," *IEEE Transactions on Circuits and Systems-I: Fundamental Theory and Applications*, vol. 44, no. 12, pp. 1129–1142, 1997.

[25] G. Yuan, S. Banerjee, E. Ott, and J.A. Yorke, "Border-collision bifurcations in the buck converter," *IEEE Transactions on Circuits and Systems-I: Fundamental Theory and Applications*, vol. 45, no. 7, pp. 707–716, 1998.

[26] J.M.T. Thompson and H.B. Stewart, "A tutorial glossary of geometrical dynamics," *International Journal of Bifurcation and Chaos*, vol. 3, no. 2, pp. 223–239, 1993.

[27] E.H. Abed, H.O. Wang, and A. Tesi, "Control of bifurcations and chaos," in *The Control Handbook*, W.S. Levine, Ed., pp. 951–966. CRC Press, 1996.

[28] R.D. Middlebrook and S. Ćuk, "A general unified approach to modelling switching-converter power stages," in *IEEE Power Electronics Specialists Conference Record*, 1976, pp. 18–34.

[29] S. Ćuk and R.D. Middlebrook, "A general unified approach to modelling switching DC-to-DC converters in discontinuous conduction mode," in *IEEE Power Electronics Specialists Conference Record*, 1977, pp. 36–57.

[30] D.C. Hamill, "Power electronics: A field rich in nonlinear dynamics," in *Nonlinear Dynamics of Electronic Systems*, Dublin, 1995.

[31] B. Lehman and R.M. Bass, "Switching frequency dependent averaged models for PWM DC-DC converters," *IEEE Transactions on Power Electronics*, vol. 11, no. 1, pp. 89–98, 1996.

[32] G.C. Verghese, M. Elbuluk, and J.G. Kassakian, "A general approach to sample-data modeling for power electronic circuits," *IEEE Transactions on Power Electronics*, vol. 1, no. 2, pp. 76–89, 1986.

[33] R. Lutz and M. Grotzbach, "Straightforward discrete modelling for power converter systems," in *IEEE Power Electronics Specialists Conference Record*, 1986, pp. 761–770.

[34] C.-C. Fang, *Sampled-Data Analysis and Control of DC-DC Switching Converters*, Ph.D. thesis, University of Maryland, College Park, 1997, available at http://www.isr.umd.edu/TechReports/ISR/1997/.

[35] J.L. Duarte, "Small-signal modelling and analysis of switching converters using matlab," *International Journal of Electronics*, vol. 85, no. 2, pp. 231–269, 1998.

[36] Y.A. Kuznetsov, *Elements of Applied Bifurcation Theory*, Springer-Verlag, New York, 1995.

[37] J. Guckenheimer and P. Holmes, *Nonlinear Oscillations, Dynamical Systems, and Bifurcations of Vector Fields*, Springer-Verlag, New York, 1983.

[38] S. Wiggins, *Introduction to Applied Nonlinear Dynamical Systems and Chaos*, Springer-Verlag, New York, 1990.

[39] N. Mohan, T.M. Undeland, and W.P. Robbins, *Power Electronics: Converters, Applications, and Design*, Wiley, New York, 1995.

[40] H.K. Khalil, *Nonlinear Systems*, Macmillan, New York, 1992.

[41] K.K. Tse and H. Chung, "Decoupled technique for the simulation of pwm switching regulators using second order output extrapolations," *IEEE Transactions on Power Electronics*, vol. 13, no. 2, pp. 222–234, 1998.

[42] K.M. Smedley, *Control Art of Switching Converters*, Ph.D. thesis, California Institute of Technology, 1990.